inter.noise 2014
MELBOURNE AUSTRALIA
16-19 NOVEMBER

The flow-induced noise of square finite wall-mounted cylinders in different boundary layers.

Ric PORTEOUS[1]; Danielle MOREAU; Con DOOLAN;Zebb PRIME

School of Mechanical Engineering, University of Adelaide, Australia

ABSTRACT

The noise generated by a finite wall-mounted cylinder (FWMC) in cross-flow is relevant to a range of applications including aircraft landing gear, heat exchangers and automobile appendages. The noise generation characteristics and mechanisms of these objects depend primarily on the aspect ratio (ratio of length to width, L/W) and the height of the incoming boundary layer, δ. This paper presents acoustic and wake measurements for six square FWMC's in two different turbulent boundary layers. The aspect ratio of the cylinders ranged from $1.94 < L/W < 13.75$ and the boundary layer heights were $\delta/W = 1.2$ and 2.4. The periodic wake and far-field acoustic characteristics of the cylinders were measured simultaneously using hotwire anemometry and a single microphone. The results show that increasing the boundary layer height increases the overall noise for $L/W \leq 8.8$ but reduces the overall noise level for $L/W > 8.8$.

Keywords: Aeroacoustics, Cylinders, Wake

1. INTRODUCTION

Square finite wall-mounted cylinders (FWMCs) are ubiquitous in a range of engineering applications including submarines, railway pantographs and aircraft landing gear. FWMC's produce complex three-dimensional flow sturctures that often generate unwanted noise. Therefore, improved understanding of the underlying noise generation mechanisms of such bodies is important.

An FWMC is shown in Figure 1. The cylinder has one end immersed in the free stream (referred to as the 'free-end') and the other end fixed to a flat surface (referred to as the cylinder-wall 'junction') so that it is subject to a developing boundary layer of height δ. The cylinder is geometrically characterised by its span, L, and its width, W. The cylinder's aspect ratio is defined as L/W.

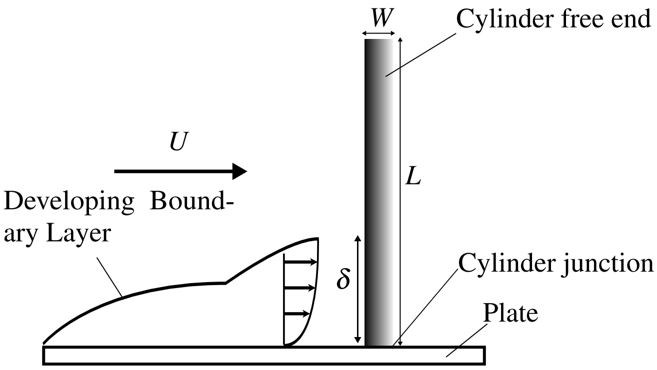

Figure 1 – An FWMC mounted to a flat plate with a width, W and length, L subject to a flow with free stream velocity, U and an incoming boundary layer height of δ.

For a semi-infinite cylinder ($L \to \infty$), the wake is characterised by the periodic shedding or vorticity in the wake of either side of the cylinder known as von Kármán vortex shedding (Gerrard 1966). The alternate shedding of vorticity occurs at a particular frequency, f_s, which is represented in non-dimensional form by the Strouhal number based on cylinder width, $St = \frac{f_s W}{U}$ where U is the free stream velocity. The vortex shedding creates a fluctuating pressure on the surface of the cylinder that creates sound (Curle 1955) that is observed

[1] ric.porteous@adelaide.edu.au

in the far-field as a tone with a frequency identical to the vortex shedding frequency (Phillips 1956). For two-dimensional sqaure cylinders, $St = 0.12$ (Blake 1986).

Moreau and Doolan (2013) experimentally studied the relationship of cylinder aspect ratio to radiated sound for square FWMCs with $1 < L/W < 14$ at Reynolds numbers based on diameter ranging from 1×10^4 to 1.4×10^4 . It was observed that for $L/W \geq 9$, two Aeolian tones existed, separated by approximately $\Delta St = 0.02$. The Strouhal numbers of both tones were lower than $St = 0.12$. Hotwire results in the wake of the cylinder revealed that the dual Aeolian tone was due to spanwise variation of the vortex shedding frequency. It was proposed that this spanwise variation was due to the formation of a cellular wake structure of vortices, similar to that observed for circular FWMCs by Farivar (1981); Ayoub and Karamcheti (1982); Gerich and Eckelmann (1982); Kawamura et al. (1984); Budair et al. (1991); Fox and Apelt (1993) and Kitagawa et al. (1999).

Becker et al. (2008) experimentally investigated the Aeolian tone generated by a square FWMC of $L/W = 6$ at Reynolds numbers ranging from 6×10^3 to 1.9×10^4 with different fore- and aft- bodies. It was found that the sound power of the aeolian tone (and therefore overall sound power level) was strongly affected by the coherency of the vortex street developed behind the cylinder. Reducing the downwash over the free-end of the cylinder allowed coherent development of vortices, increasing overall noise levels. Conversely, introducing upstream instabilities via a forebody significantly reduced the spanwise correlation of the vortices, reducing overall noise levels.

Becker et al. (2008) showed the flow-induced noise characteristics are related to the structure of coherent vortices in the wake of the FWMC which, as Moreau and Doolan (2013) demonstrated, is strongly related to the aspect ratio of the cylinder. Apart from the aspect ratio, the ratio of plate boundary layer height to width of the cylinder can also change this wake structure (Hosseini et al. 2013; Bourgeois et al. 2011). The aim of this paper is therefore to experimentally investigate the influence of aspect ratio and boundary layer height on the flow-induced noise of a square FWMC.

2. EXPERIMENTAL SETUP

2.1 Wind Tunnel Facility

The experiment was conducted in the University of Adelaide's open-jet anechoic wind tunnel. The testing is performed in an anechoic room that has internal dimensions of $1.4 \times 1.6 \times 1.8$ m. The jet nozzle is rectangular with a height of 75 mm and a width of 275 mm. The maximum flow velocity of the free-jet is approximately 32.4 m/s and the free-stream turbulence is 0.33 %.

2.2 Test Models

Six square FWMCs were mounted (one at a time) perpendicularly on a flat plate which was flush mounted to the jet nozzle, as shown in Figure 2. The flat plate measured 300×155 mm. The cylinders were square with a width, $W = 9.95$ mm, and length, L, ranging from 19.3 mm to 135.95 mm corresponding to an aspect ratio, L/W, of 1.94, 3.89, 5.85, 8.81, 11.86 and 13.75.

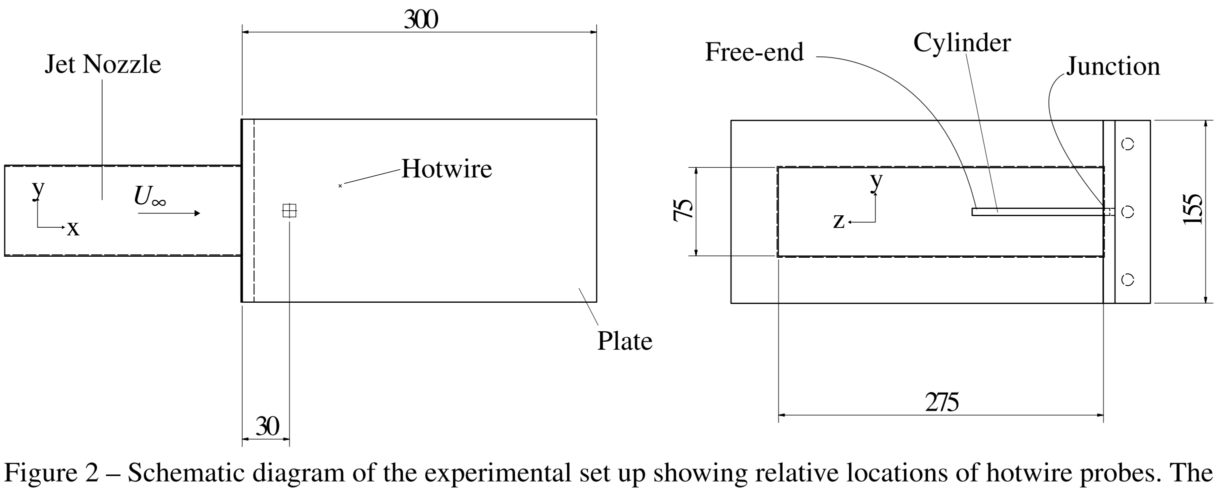

Figure 2 – Schematic diagram of the experimental set up showing relative locations of hotwire probes. The coordinate system used is shown in the diagram.

2.3 Measurement Equipment and Procedure

A TSI 1261A miniature boundary layer hotwire probe was used to measure the incoming boundary layer characteristics. The probe had a wire length of 1.27 mm and a wire diameter of 3.81 μm. The boundary layer profile was measured at the location of the cylinder with the cylinder removed. To do this, the hotwire probe was connected to a Dantec automatic traverse with 6.25 μm accuracy allowing the hotwire to be traversed perpendicular to the plate. The hotwire was connected to a TSI IFA 300 Constant Temperature Anemometry system. The CTA system was used in conjunction with Thermal Pro software to automatically optimise the frequency response of the CTA circuit.

Single wire hotwire anemometry was also used to measure the fluctuating velocity in the wake of the cylinders. For this set-up, a TSI 1260A miniature straight probe with the same wire dimensions and control software as the boundary layer probe was used. As shown in Figure 2, the probe was located 4D downstream (the x-direction) from the cylinder and 2D laterally (the y-direction) from the cylinder. According to Rostamy et al. (2013) this location is outside of the reverse flow region of the wake. The hotwire was connected to the traverse so that it could be moved to positions along the span of the cylinder (the z-direction). For each measurement, the hotwire was moved to 10 equally spaced points along the cylinder span, starting from the free-end.

Acoustic measurements were taken with a single G.R.A.S 40PH 1/4" microphone located 0.5 m directly above the cylinder. The microphone's frequency range is ± 1 dB between 50-5000 Hz as stated in the transducer documentation.

The experiment was run at a free-stream velocity of 32 m/s, producing a Reynolds number based on cylinder width of 2×10^4. For every hotwire measurement, the microphone simultaneously measured acoustic pressure fluctuations. Velocity and acoustic pressure fluctuations were sampled for 10 seconds at 2^{16} Hz using a DAQ with an automatic anti-aliasing filter.

3. BOUNDARY LAYER

Two different boundary layers were used in this investigation; a low thickness turbulent boundary layer (LTB) that was allowed to develop naturally out of the wind tunnel nozzle and a high thickness turbulent boundary layer (HTB) produced using an upstream tripping rod to thicken the boundary layer. The upstream tripping rod was 4 mm in diameter and located 18 cylinder widths upstream from the cylinder location.

Figure 3 compares the two boundary layer velocity profiles and turbulent intensity profiles at the position of the cylinder axis (with the cylinder removed). Table 1 compares the boundary layer thickness, δ_{99}, displacement thickness, δ^*, momentum thickness, θ^*, shape factor, $H = \delta^*/\theta$ and $Re_\tau = \dfrac{\delta_{99} u_\tau}{\mu}$, where u_τ is the friction velocity of the two boundary layers. The results are normalised by the cylinder width, W, where appropriate. The friction velocity was estimated by using curve fitting method of Coles (1968).

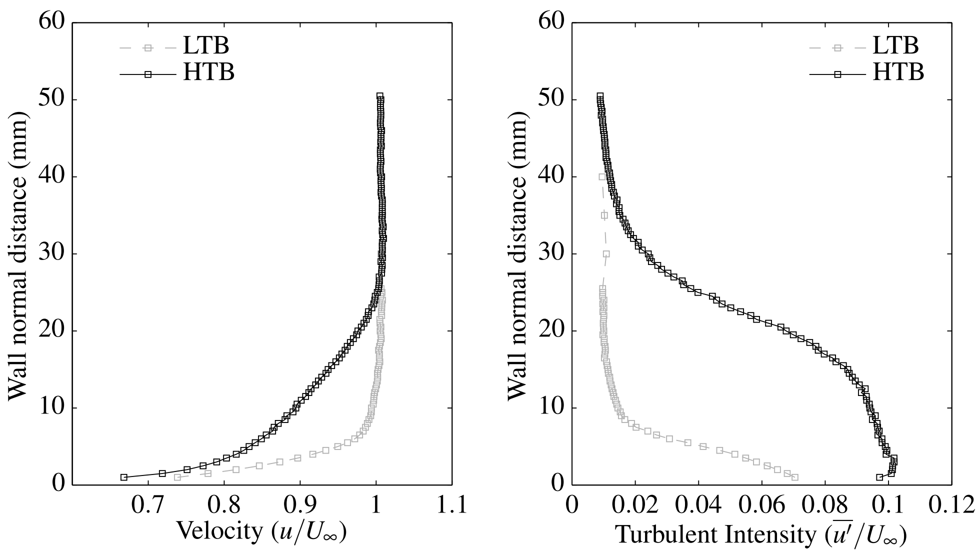

Figure 3 – Mean and turbulent velocity profiles of the LTB and HTB.

Figure 3 shows that the HTB was significantly thicker than the LTB; the LTB had a thickness of 1.21D

	δ_{99}/D	δ^*/D	θ/D	H	u_τ
LTB	1.2	0.09	0.04	1.5	1142
HTB	2.36	0.23	0.18	1.3	1946

Table 1 – Comparison of key boundary layer characteristics between the LTB and the TTB, normalised by cylinder width where appropriate.

while the HTB had a thickness of $2.36D$. The shape factors of the two boundary layers indicate that they were both close to fully-developed. As shown in Figure 3, HTB had a significantly higher turbulent intensity than the LTB.

4. ACOUSTIC CHARACTERISTICS

4.1 Overall sound pressure level

Figure 4a shows the change in overall sound pressure level (OASPL) in with cylinder aspect ratio for the LTB and HTB cases while Figure 4b shows the difference in OASPL between the two cases (i.e HTB-LTB). The values are calculated based on time series data bandpassed between 200 Hz and 10000 Hz. In both boundary layers, the OASPL increases with the length of the cylinder. For $L/W \leq 8.8$, the OASPL is lower for the LTB than the HTB. However, as the cylinder aspect ratio increases above 8.8, the OASPL of the LTB case is higher than that of the HTB case.

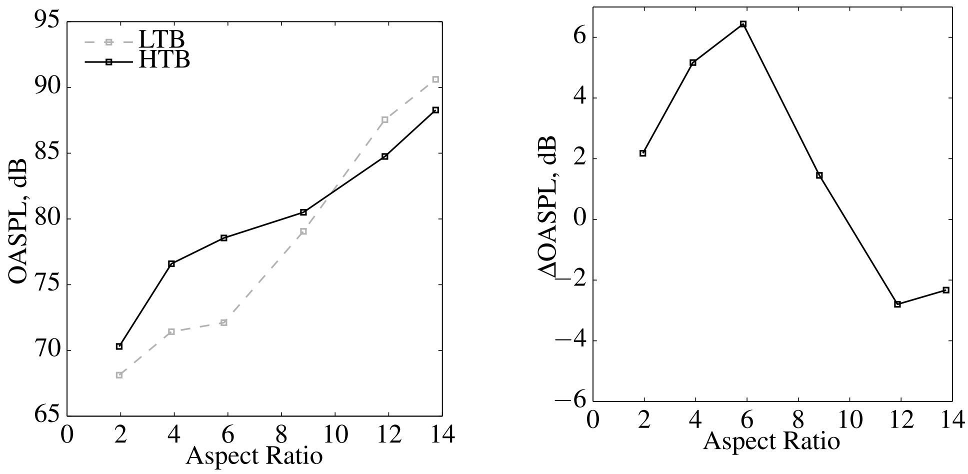

(a) Change in overall sound pressure level with L/W.

(b) Difference in overall sound pressure level between HTB and LTB.

Figure 4 – Change in overall sound pressure level (OASPL) with aspect ratio in the LTB and HTB. Figure 4b highlights the difference in OASPL between the two cases.

4.2 Narrow band spectra

Figure 5 compares the power spectral density (PSD) of acoustic pressure fluctuations for the LTB and HTB cases for each cylinder aspect ratio. These were calculated with Welch's averaging method using 38 blocks of length 2^{15} samples with a Hanning window and 50% overlap. This gave a spectral resolution of 2 Hz ($\Delta St = 6.25 \times 10^{-4}$).

Figures 5b and 5c show that the HTB is characterised by a broad peak centered at $St = 0.1$ for $3.89 \leq L/W \leq 8.8$, where a strong tone due to vortex shedding occurs for the LTB case. Because a definite peak is still evident, this suggests that vortex shedding still occurs in the HTB case, albeit with a higher amount of frequency jitter. Contrastingly, in Figure 5a for the case of $L/W = 1.94$, the small vortex shedding peak observed in the LTB case is completely replaced with a broadband signal, suggesting that no organised vortex shedding is occurring. The HTB also increases broadband noise levels above $St = 0.2$ for these aspect ratio cylinders. The increase in broadband noise levels explains the increase in OASPL for these aspect ratios.

For cylinders with $L/W \geq 11.86$, the broadband noise levels above $St = 0.2$ are similar in magnitude for both boundary layers. The primary affect of the HTB is on the two vortex shedding peaks at $St = 0.122$ and

0.095 respectively. For $L/W = 11.86$, the higher frequency tone has a lower magnitude by approximately 6 dB/Hz and occurs at a slightly lower frequency with $\Delta St = St_{LTB} - St_{HTB} = 0.007$. The lower frequency tone is also reduced by 2.3 dB/Hz in magnitude but occurs at the same frequency. For $L/W = 13.75$, the higher frequency tone is again at a reduced magnitude by 6 dB/Hz for the HTB and occurs at a lower frequency with $\Delta St = 0.003$. The lower frequency tone has identical magnitude and frequency in both the LTB and HTB cases. The reduction in magnitude of the higher frequency tone level for the HTB spectra explains the decrease in OASPL (shown in Figure 4) for these cases.

5. FLUCTUATING VELOCITY SPECTRA

Figures 6 and 7 show the fluctuating velocity power spectral density as a function of normalised cylinder length, z/L, for the two boundary layer cases.

The fluctuating velocity spectra are comprised of two components; a narrowband high magnitude peak associated with vortex shedding and a wider bandwidth ('wideband') lower magnitude hump associated with random turbulence at a range of different length scales.

Figures 6a, 6c, 6e, 7a, 7c and 7e show that for the LTB, vortex shedding occurs for all cylinder aspect ratios as evidenced by the strong peak in velocity fluctuations at $0.1 < St < 0.14$. The bandwidth of this peak is very narrow across the entire cylinder span. At $L/W > 8.8$, the dominant frequency along the span splits into two peaks. The higher frequency peak emanates from the junction region and extends to approximately $z/L = 0.9$. The lower frequency peak originates at approximately $z/L = 0.4$ and extends to the free-end $z/L = 1$.

Accompanying the vortex shedding peak are the wideband velocity fluctuations of lower magnitudes than the vortex shedding fluctuations, but higher than the free-stream (free-stream turbulence levels are indicated by blue regions in the Figures 6 and 7). For $L/W \leq 5.85$ these wideband fluctuations are strongest near the junction region and steadily reduce in bandwidth and magnitude towards the free-end. For $L/W = 1.94$, the wideband fluctuations continue to approximately $z/L = 0.5$ and for $L/W = 3.89$ and 5.84 they continue until $z/L = 0.8$. For $L/W \geq 8.8$ the spanwise distribution of wideband velocity fluctuations is different to that for cylinders of lower aspect ratio. These cylinders experience constant bandwidth wideband fluctuations until $z/L = 0.8$ to 0.9, after which the wideband fluctuations experience a sudden drop in magnitude.

Figure 6b shows that in the HTB case, for $L/W = 1.9$, there is no narrow band peak associated with vortex shedding. Instead, wideband velocity fluctuations exist at a centre frequency of $St = 0.1$ across the entire cylinder span. This is consistent with the results of Figure 5a, where it was concluded that no organised vortex shedding occurred at this aspect ratio in the HTB. As the aspect ratio increases from $L/W = 1.9$ to $L/W = 5.84$ (see Figures 6d and 6f), a narrow band peak associated with vortex shedding forms across the span of the cylinder at $St = 0.1$. For these aspect ratios the bandwidth of wideband fluctuations deceases near the free-end. At $L/W \geq 8.8$, the velocity fluctuation spectral map is similar for both boundary layers. As for the LTB case, when $L/W = 11.86$, the vortex shedding frequency splits along the span (see Figure 7d and 7f). However for the HTB case, vortex shedding at the junction is shifted to a slightly lower frequency.

6. CONCLUSIONS

This paper has presented an experimental investigation that explores the influence of the aspect ratio of a square FWMC and the height of the incoming boundary layer on the flow-induced noise characteristics of the cylinder. The results show that both the aspect ratio and the boundary layer height can affect the overall sound pressure level of the flow-induced noise. As aspect ratio increase, the OASPL increases. The relationship with boundary layer height is more intriguing. It is shown that there exists a certain aspect ratio, in this case $L/W \approx 8.8$, where the OASPL will decrease as the boundary layer height increases. Along with OASPL, narrow band acoustic spectra and narrow band velocity spectra along the span have been presented. These results have shown that the boundary layer height and turbulent characteristics has a profound effect on the nature of the fluctuating wake behind the cylinder and spectral characteristics of the flow-induced noise.

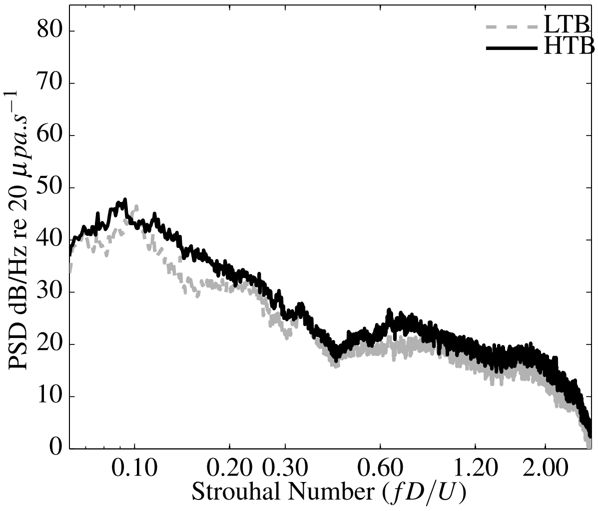

(a) Comparison of PSD for square cylinders of L/D=1.94.

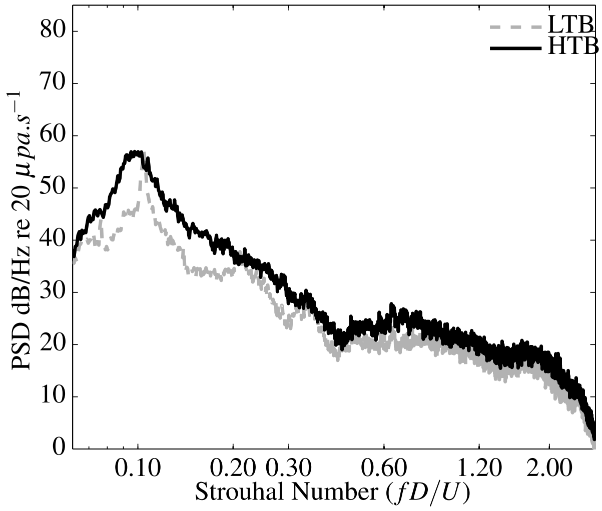

(b) Comparison of PSD for square cylinders of L/D=3.89.

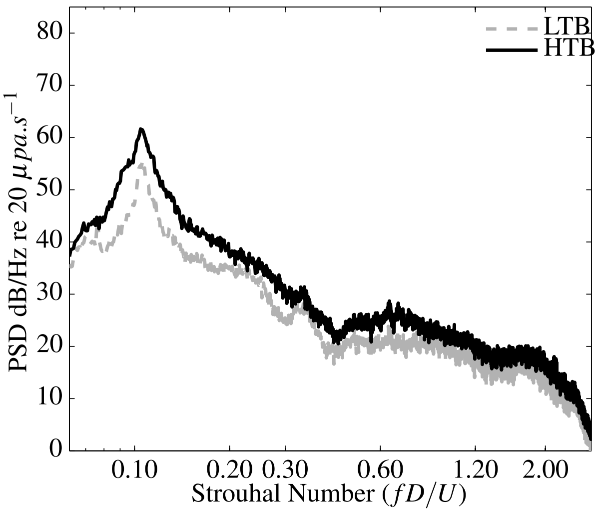

(c) Comparison of PSD for square cylinders of L/D=5.85.

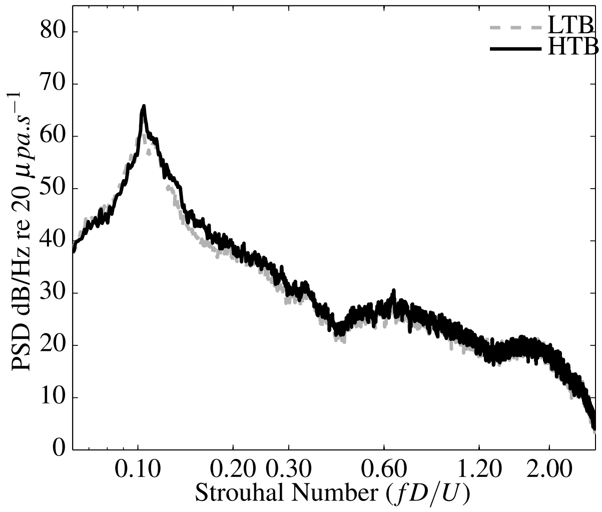

(d) Comparison of PSD for square cylinders of L/D=8.81.

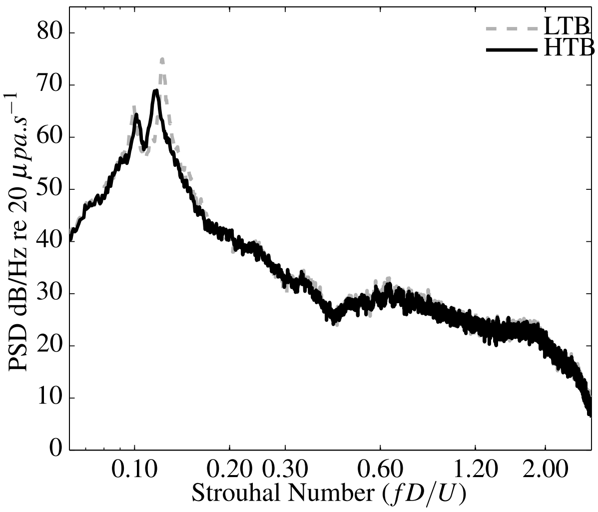

(e) Comparison of PSD for square cylinders of L/D=11.86.

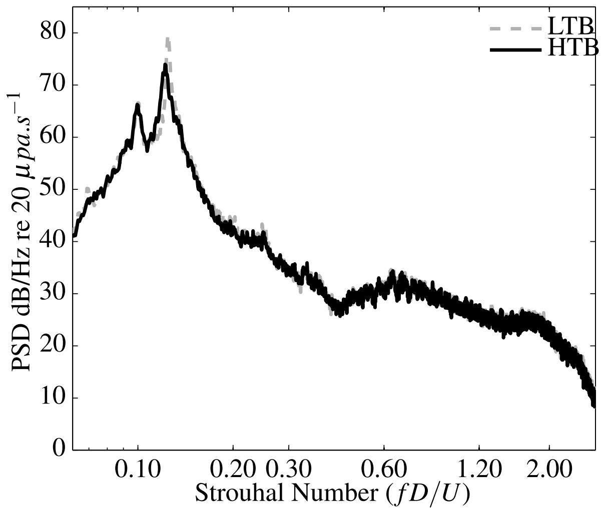

(f) Comparison of PSD for square cylinders of L/D=13.75.

Figure 5 – Comparison of far-field acoustic power spectral density between LTB and HTB cases for different aspect ratios.

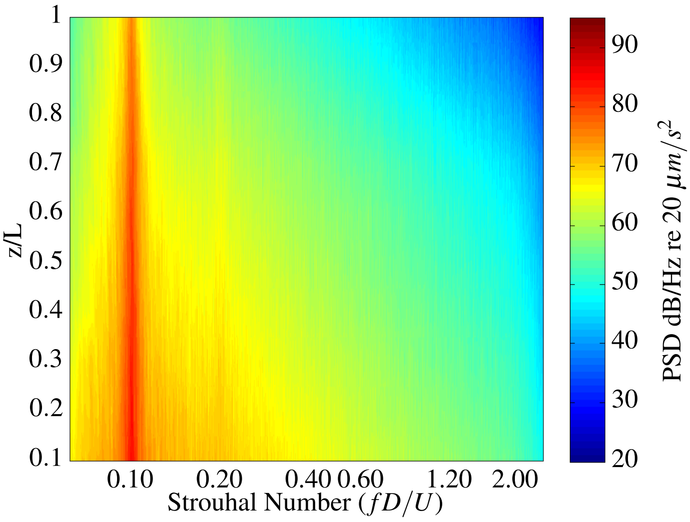

(a) Power spectral density of the fluctuating velocity in the LTB case for L/D=1.94.

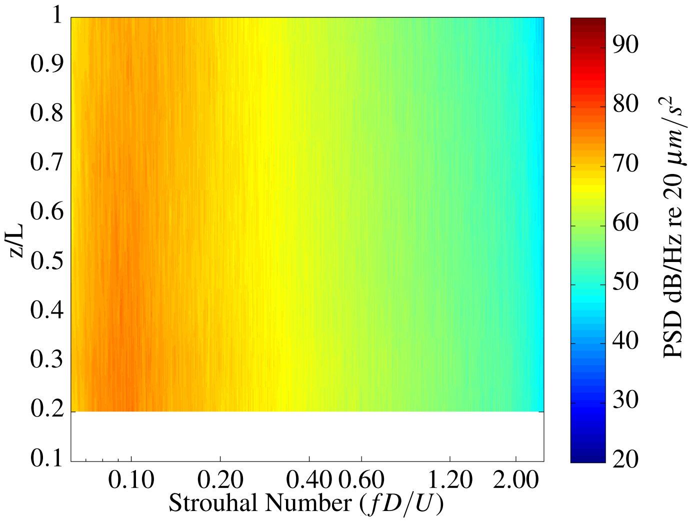

(b) Power spectral density of the fluctuating velocity in the HTB case for L/D=1.94.

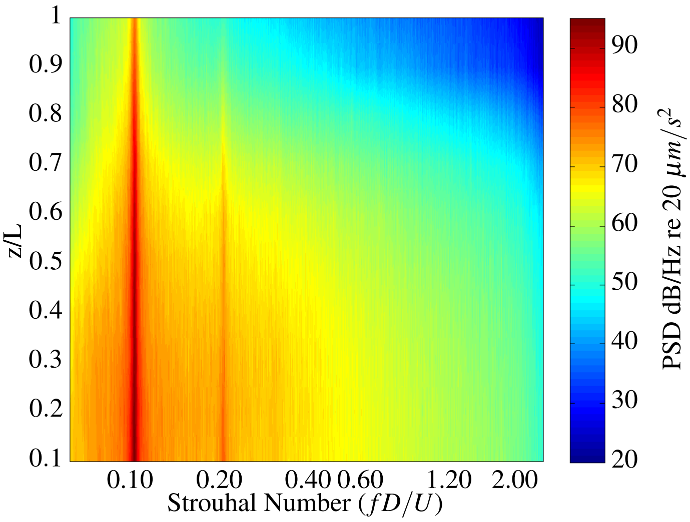

(c) Power spectral density of the fluctuating velocity in the LTB case for L/D=3.89.

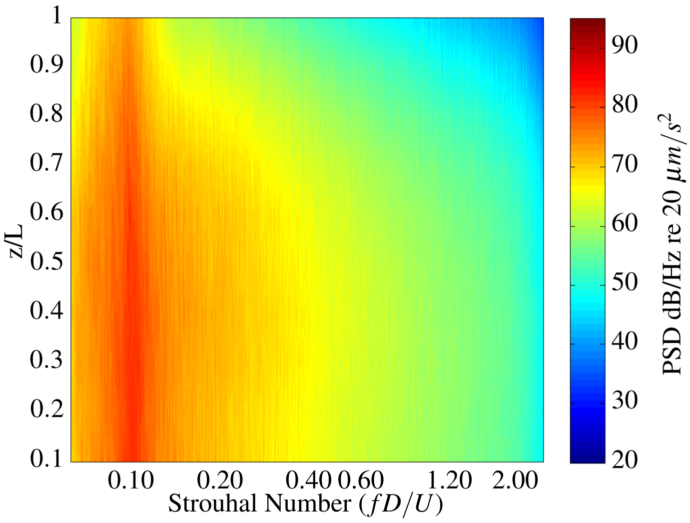

(d) Power spectral density of the fluctuating velocity in the HTB case for L/D=3.89.

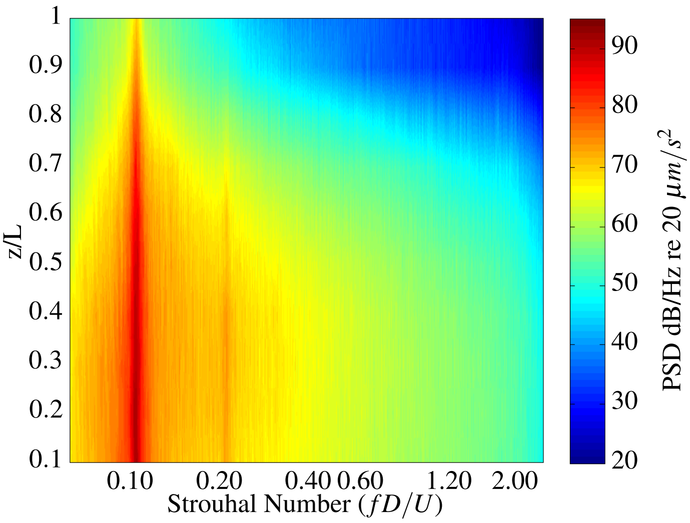

(e) Power spectral density of the fluctuating velocity in the LTB case for L/D=5.85.

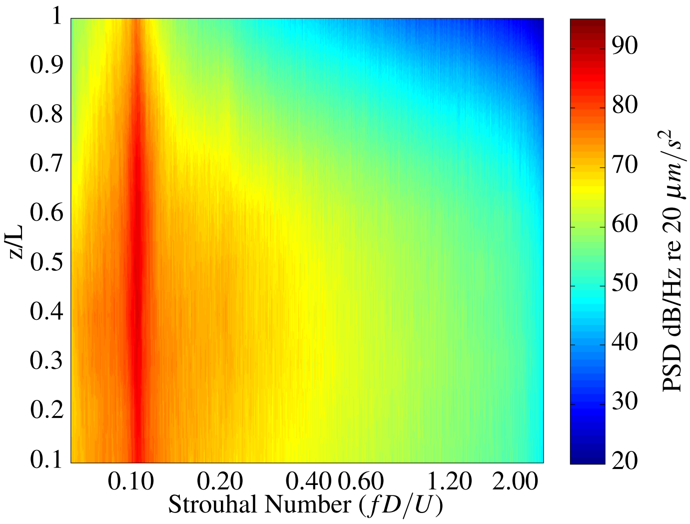

(f) Power spectral density of the fluctuating velocity in the HTB case for L/D=5.85.

Figure 6 – Spectral maps of the fluctuating velocity for $L/W = 1.94$ to 5.85 for the LTB case (left) and HTB case (right).

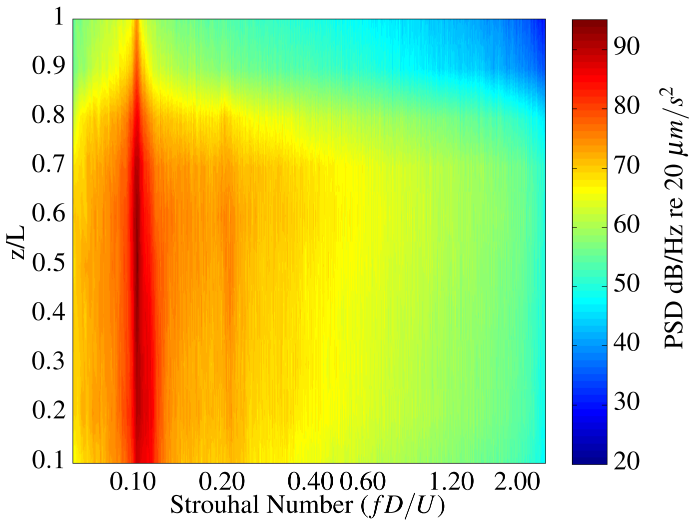

(a) Power spectral density of the fluctuating velocity in the LTB case for L/D=8.81.

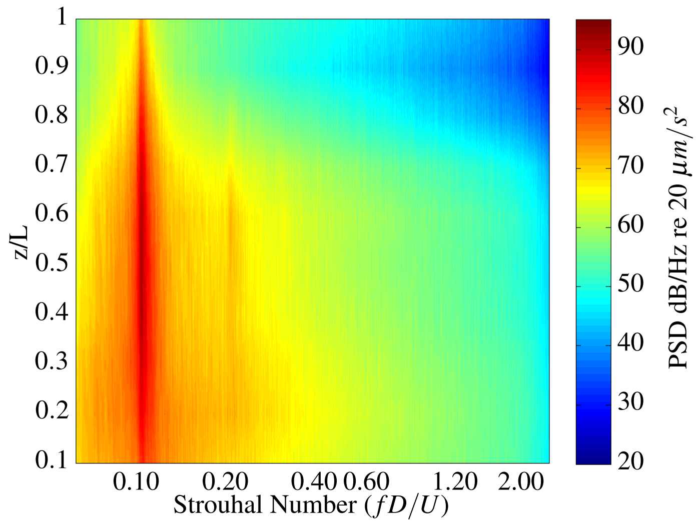

(b) Power spectral density of the fluctuating velocity in the HTB case for L/D=8.81.

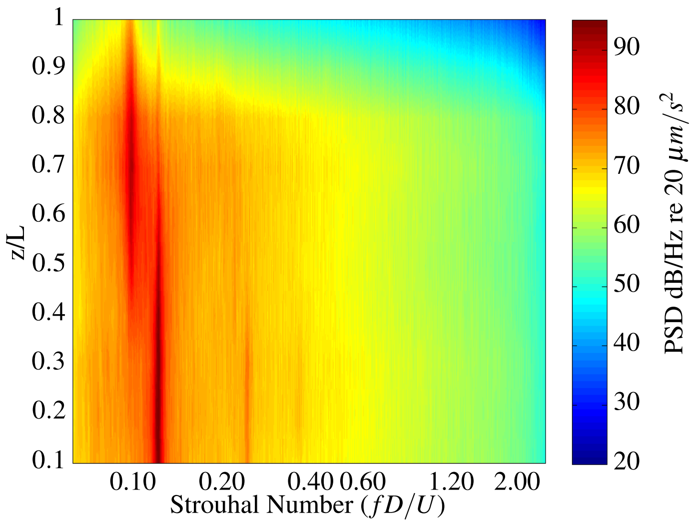

(c) Power spectral density of the fluctuating velocity in the LTB case for L/D=11.86.

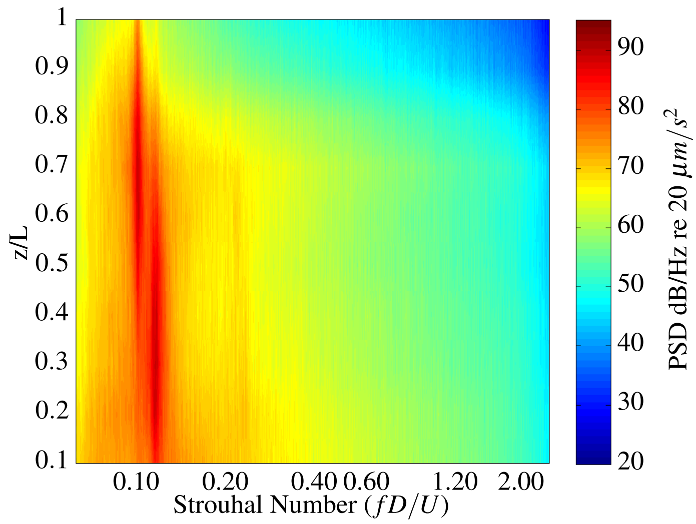

(d) Power spectral density of the fluctuating velocity in the HTB case for L/D=11.86.

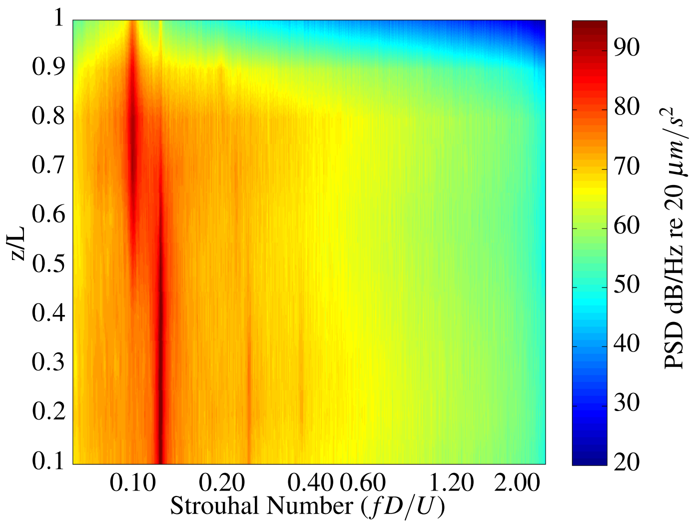

(e) Power spectral density of the fluctuating velocity in the LTB case for L/D=13.75.

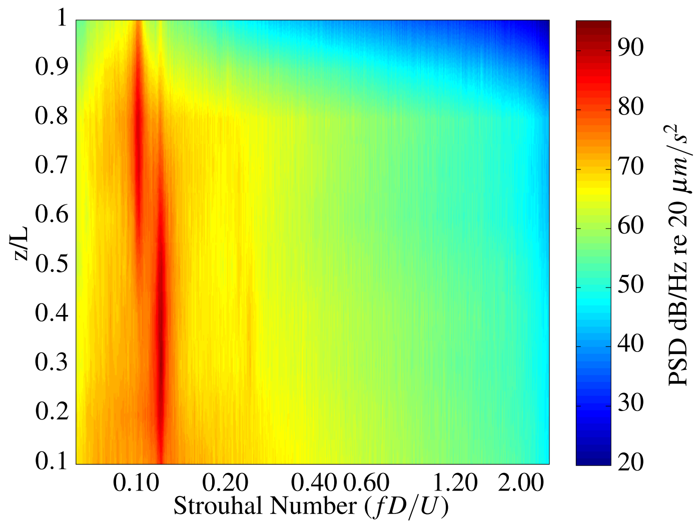

(f) Power spectral density of the fluctuating velocity in the HTB case for L/D=13.75.

Figure 7 – Spectral maps of the fluctuating velocity for $L/W = 8.81$ to 13.75 for the LTB case (left) and HTB case (right).

REFERENCES

Ayoub, A. and K. Karamcheti (1982). "An experiment on the flow past a finite circular cylinder at high subcritical and supercritical Reynolds numbers". In: *Journal of Fluid Mechanics* 118, pp. 1 –26. DOI: 10.1017/S0022112082000937 (cit. on p. 2).

Becker, S., C. Hahn, M. Kaltenbacher, and R. Lerch (2008). "Flow-induced sound of wall-mounted cylinders with different geometries". In: *AIAA Journal* 46.9, pp. 2256–2281. DOI: 10.2514/1.34865 (cit. on p. 2).

Blake, W. K. (1986). *Mechanics of flow-induced sound and vibration, volume 1, general concepts and elemetary sources*. Ed. by Frenkiel, F. N. Academic Press (cit. on p. 2).

Bourgeois, J., P. Sattari, and R. Martinuzzi (2011). "Alternating half-loop shedding in the turbulent wake of a finite surface-mounted square cylidner with a thin boundary layer". In: *Physics of Fluids* 23.9, p. 095101. DOI: 10.1063/1.3623463 (cit. on p. 2).

Budair, M., A. Ayoub, and K. Karamcheti (1991). "Frequency measurements in a finite cylinder wake at a subcritical Reynolds number". In: *AIAA Journal* 29.12, pp. 2163 –2168. DOI: 10.2514/3.10854 (cit. on p. 2).

Coles, D. (1968). "The young person's guide to the data". In: *Proceedings Computation of Turbulent Boundary Layer- 1968 AFOSR-IPF-Stanford Conference*. Vol. 2. Stanford University (cit. on p. 3).

Curle, N. (1955). "The influence of solid boundaries upon aerodynamic sound". In: *Proceedings of the Royal Society of London. Series A, Mathematical and Physical Sciences* 231.1187, pp. 505–514. DOI: 10.1098/rspa.1955.0191 (cit. on p. 1).

Farivar, D. (1981). "Turbulent uniform flow around cylinders of finite length". In: *AIAA Journal* 19.3, pp. 275 –281. DOI: 10.2514/3.7771 (cit. on p. 2).

Fox, T. A and J. Apelt (1993). "Fluid-induced loading of cantilevered circular cylinders in a low-turbulence uniform flow Part 3: fluctuating loads with aspect ratios 4 to 25". In: *Journal of Fluids and Structures* 7.4, pp. 375 –386. DOI: 10.1006/jfls.1993.1022 (cit. on p. 2).

Gerich, D. and H. Eckelmann (1982). "Influence of end plate and free ends on the shedding frequency of circular cylinders". In: *Journal of Fluid Mechanics* 122, pp. 109 –121. DOI: 10.1017/S0022112082002110 (cit. on p. 2).

Gerrard, J. H. (1966). "The mechanics of the formation region of vortices behind bluff bodies". In: *Journal of Fluid Mechanics* 25, pp. 401 –413. DOI: 10.1017/S0022112066001721 (cit. on p. 1).

Hosseini, Z., J. A. Bourgeois, and R. J. Martinuzzi (2013). "Large-scale structure in dipole and quadrupole wake of a wall-mounted finite rectangular cylinder". In: *Experiments in Fluids* 54. DOI: 10.1007/s00348-013-1595-2 (cit. on p. 2).

Kawamura, T., M. Hiwada, T. Hibino, I. Mabuchi, and M. Kumada (1984). "Flow around a finite circular cylinder on a flat plate (Cylinder height greater than turbulent boundary layer thickness)". In: *Bulletin of Japan Society of Mechanical Engineers* 27.232, pp. 2142 –2151 (cit. on p. 2).

Kitagawa, T., Y. Fujino, and K. Kimura (1999). "Effects of free-end conditions on end-cell-induced vibration". In: *Journal of Fluids and Structures* 13.4, pp. 499–518. DOI: 10.1006/jfls.1999.0214 (cit. on p. 2).

Moreau, D. and C. J. Doolan (2013). "Flow-induced sound of wall-mounted finite length cylinders". In: *AIAA Journal* 51.10, pp. 2493 –2502. DOI: 10.2514/1.J052391 (cit. on p. 2).

Phillips, O. (1956). "The intensity of Aeolian Tones". In: *Journal of Fluid Mechanics* 1.6, pp. 607 –624. DOI: 10.1017/S0022112056000408 (cit. on p. 2).

Rostamy, N., D. Sumner, D. Bergstrom, and J. Bugg (2013). "Instantaneous flow field above the free end of finite-height cylinders and prisms". In: *International Journal of Heat and Fluid Flow* 43, pp. 120–128. DOI: 10.1016/j.ijheatfluidflow.2013.04.005 (cit. on p. 3).